Electronic and optical properties of vanadium oxides from first principles

N.J. Szymanski [a], Z.T.Y. Liu [a], T. Alderson [a], N.J. Podraza [a], P. Sarin [b], S.V. Khare [a,*]

[a] Department of Physics and Astronomy, University of Toledo, Toledo, OH 43606, USA
[b] School of Materials Science and Engineering, Oklahoma State University, Tulsa, OK 74106, USA

ARTICLE INFO

ABSTRACT

We have studied the structural, energetic, electronic, and optical properties of six compounds belonging to the system of vanadium oxides (VO_2, V_2O_5, V_2O_3, V_3O_5, V_4O_7, and V_6O_{13}), including both high- and low-temperature phases, obtained using first principles calculations based on density functional theory. The optimized structure of each compound is found to display strong octahedral distortion. This has a major impact on the electronic structures, causing strong mixing of t_{2g} and e_g orbitals. The electronic density of states was calculated with hybrid HSE06 functionals and the GGA + U method. The results show that the HSE06 functionals provide band gap values consistent with available experimental data. For the high-temperature phase of V_2O_5, we predict a band gap of 2.32 eV. Charge transfer is shown to decrease monotonically as a function of V-O ratio for all compounds. Complex dielectric functions, as computed with hybrid functionals and the GGA + U method, are reported. Hybrid functionals overestimate the energies at which absorption peaks occur, indicating strong electron-hole interaction and lattice polarization within the system. The computed optical conductivity, as derived from optical properties found with the GGA + U method, is in good quantitative agreement with available experimental data. The theoretical framework developed is applicable for other vanadium oxide phases and similar transition metal oxides.

1. Introduction

Transition metal oxides have long been an area of great interest [1]. Due to their unique physical, thermal, and electronic properties, these materials have varied applications in gate dielectrics, transparent conducting oxides, and thin-film transistors [2]. Vanadium oxides are of particular interest, as they provide a unique advantage for many optoelectronic devices, such as "smart" windows [3], thermal sensors [4], and resistive random access memories [5]. This system has received extensive attention due to its versatile characteristics, such as the metal-insulator transition (MIT) which occurs in some of these compounds. The MIT can be induced by pressure and/or temperature, causing the materials to undergo changes in structural, electronic, and optical properties [6].

These reversible phase transitions make vanadium oxides reasonable model systems to explore both theoretically and experimentally. Many experimental works have been conducted to study the characteristics of vanadium oxides in both their high- and low-temperature phases. Thus far, VO_2, V_2O_5, V_2O_3, V_3O_5, V_4O_7, and V_6O_{13} have received the most experimental interest [7–27]. For these six compounds, structural properties are

well-known over the MIT, with lattice constants and internal parameters reported [7–17]. Their electronic structures have been widely studied, and experimental band gaps have been reported for each, with the exception of the high-temperature phase of V_2O_5 [18–23]. Optical conductivities have been determined for these compounds (except for high-temperature V_2O_5), however, the data remains relatively limited, with values known only for low frequencies [22,24–27]. Also, direction-dependent complex dielectric functions are not well-known for these vanadium oxides. Lastly, electronic charge transfer is a potentially important property which has not yet been systematically studied for these systems, and no detailed values have been reported.

Theoretically, these materials have presented a challenge, as strongly correlated materials have been known to cause problems for standard *ab initio* techniques [28]. However, to remedy this difficulty, a variety of advanced theoretical techniques have been implemented to study vanadium oxides. The DFT + U formalism has been successful in describing the electronic structure for VO_2 [5], V_2O_3 [5], V_6O_{13} [29], and V_4O_7 [30], each in their high- and low-temperature phase; however, the accuracy of band gap prediction is strongly dependent on the chosen *U*-value. Hybrid functionals and the GW method have been used to predict electronic structures and band gaps for both phases of VO_2 [31,32], V_2O_3 [33,34], and V_2O_5 [35,36], the results of which agree relatively well

* Corresponding author.
   E-mail address: sanjay.khare@utoledo.edu (S.V. Khare).

with experiment. Only for VO_2 and V_2O_5 have optical spectra been computed using hybrid functionals [31,32] and the GW [35] approximation respectively. Both have provided qualitatively satisfactory results, however, for each compound, the computed energies at which the dielectric features occur were shifted to the higher energy range. This effect has been suggested to be caused by strong electron-hole interaction and lattice polarization [31,35]. Thus, a systematic investigation of the efficacy of advanced theoretical methods, such as GGA+U and hybrid functionals, for computing electronic and optical properties of vanadium oxides is missing. This work seeks to fill this gap in the literature

Here, we have investigated the properties of VO_2, V_2O_5, V_2O_3, V_3O_5, V_4O_7, and V_6O_{13}. We present a complete theoretical description of their structural, energetic, electronic, and optical properties in both their high- and low- temperature phases. The main conclusions from this work are: (i) The structure of each compound is found to display strong octahedral distortion, which leads to strong mixing of the t_{2g} and e_g orbitals. (ii) Charge transfer is directly related to the underlying structural characteristics, and is shown to decrease monotonically as a function of V-O ratio. (iii) Hybrid functionals accurately predict band gaps but yield optical spectra which overestimate the photon energies of absorption peaks, indicating strong electron-hole interaction and lattice polarizations within these phases. (iv) The DFT + U method provides prediction of optical spectra which match well with experimental data.

2. Computational methods

All density functional theory (DFT) calculations have been implemented using the Vienna *Ab initio* Simulation Package (VASP) [37–40]. The V_sv potential, which includes the semi-core *s* and *p* electrons, was used for vanadium, while the default potential was used for oxygen. Additionally, a plane wave cutoff energy of 400 eV was used throughout the computations. All k-point meshes consisted of at least 1000 k-points per reciprocal atom (KPPRA). Gaussian smearing with a sigma value of 0.05 eV was used. Spin polarization has also been considered in order to account for the magnetic ordering of the compounds. A convergence criterion of 10^{-4} eV was chosen for all electronic iterations.

We chose the low- and high-temperature structures for each compound from experimental results reported in the literature [7–17]. We then optimized each structure to its lowest energy state using the Purdew-Burke-Ernzerhoff (PBE) generalized gradient approximation (GGA) [41,42]. The unit cell shape, volume, and ionic positions were allowed to relax until the force acting on each atom was less than or equal to 0.01 eV/Å [43]. We have found that for V_3O_5, V_4O_7, and V_6O_{13}, the optimization of the high-temperature structure results in approximately the same cell shape and ionic positions as the low-temperature phase. This behavior is most likely because for these three compounds, the differences in geometry occurring over the MIT are relatively small. Therefore, we have relaxed the low-temperature phase of V_3O_5, V_4O_7, and V_6O_{13}. For the high-temperature phase, we fixed the experimental lattice constants, positioned the atoms in their experimental configurations [13,15,16], and relaxed all internal degrees of freedom. Thus, the experimentally reported structural geometry was retained after full relaxation. For VO_2, V_2O_5, and V_2O_3, the structural differences between the high- and low-temperature phases are substantial enough that we were able to relax both phases completely, including lattice constants, while maintaining geometries similar to the respective experimentally determined structure. The resultant structures were used throughout the remainder of the calculations.

The formation energy of each compound was computed through implementation of GGA. High-precision static calculations

were performed in order to obtain an accurate final energy. Using this value, we found the formation energy by calculating the difference between the energy of the V_xO_y compound and the energies of its constituents in their ground states. Accordingly, the following equation was used: $E_{Form} = E(V_xO_y) - xE(V) - yE(O_2)/2$. Furthermore, for consistency of comparison between different compounds, we calculated $E_{norm} = 2E_{Form}/y$, which is what is reported in the results.

Next, the electronic charge transfer was calculated for both the high- and low-temperature phase of each compound. This calculation was done by using Bader's analysis [44] to find the charge density corresponding to each individual atom within the compound. From this data, the average charge transfer from oxygen to vanadium was determined.

To study the electronic and optical properties, we implemented two methods: the Heyd-Scuseria-Ernzerhof hybrid functional (HSE06) and the GGA + U scheme. For the latter method, we have chosen to implement the approach developed by Dudarev et al. [45]. In this approach, a self-energy correction term, which depends on given *U*- and *J*-values, is computed and added to the standard GGA energy. However, for this approach, only the difference between *U* and *J* is meaningful ($U_{eff} = U - J$) [45]. Previous works have shown that results vary substantially depending on the magnitude of the *U* and *J* of choice [5,29,30,46,47]. In this work, we have set *U* = 3.25 eV and *J* = 0.0 eV, so that the effective *U*-value (U_{eff}) is equal to 3.25 eV. These values are in accordance with the results found by Wang et al. [48]. We have applied the self-energy correction term to the *d* orbitals of vanadium [49]. By implementing these methods within VASP, the electronic density of states was computed of each compound. We have also obtained the energy-dependent complex dielectric function ($\varepsilon = \varepsilon_1 + i\varepsilon_2$) [50,51]. Complex optical conductivity spectra (σ) are determined from spectra in ε, with the real part of the optical conductivity calculated by [52]:

$$Re\ \sigma(\omega) = (\omega\varepsilon_2)/(4\pi).$$

3. Results and discussion

3.1. Structure details

The compounds under study display a wide variety of lattice types and space groups, as listed along with lattice constants and angles in Table 1. There is good agreement between our computed structural unit cell parameters and experimentally measured values from the literature where available. Slight deviations consistent with those expected from the application of the GGA method [53,54] are observed. Previous theoretical studies on various vanadium oxides provide relaxed cell parameters which agree with our results. Two works [5,55] regarding the high-temperature phase of V_2O_3 have reported that structural optimization resulted in a noticeable increase of the *c*-axis length and small decreases of *a*- and *b*-axes, with which our results agree. A separate study [36] on low-temperature V_2O_5 noticed similar effects, in which the longest axis of the unit cell increased and the remaining two axes decreased. Our calculated lattice parameters for V_2O_5 are consistent with this result. A recent work [56] has studied VO_2, V_2O_3, and V_2O_5 through the implementation of the local density approximation (LDA). Their calculated lattice parameters show overall agreement with our work, although some there is some differences in the V_2O_3 cell size and shape. These differences are well understood due to the different approximations (GGA vs. LDA) used [57].

Fig. 1 shows visual representations of each crystal structure. At first glance, all compounds appear to consist of VO_6 octahedra. However, for many of the compounds, the octahedra exhibit

Table 1
Unit cell structures for each compound in both the high- and low-temperature phase, represented by "HT" and "LT". Our calculated values of structural parameters are shown. For comparison, experimental parameters are listed in parentheses. For structures which have equivalent *a*- and *b*-values, "-" is listed for *b*. All compounds have been structurally optimized, with the exception of V_3O_5, V_4O_7, and V_6O_{13} in their high-temperature phases, where experimental lattice constants were used. It was determined that relaxation of these phases resulted in approximately the same cell shape and ionic positions as the low-temperature phase. Thus, we have used experimental configurations for these three high-temperature phases.

Compound	Phase	Lattice type	Space group	a (Å)	b (Å)	c (Å)	α, β, γ (°)
VO_2[a]	HT	Tetragonal	$P4_2/mnm$	4.542 (4.530)	–	2.826 (2.869)	90.00 (90.00)
VO_2[b]	LT	Monoclinic	$P2_1/c$	5.662 (5.742)	4.532 (4.517)	5.346 (5.375)	122.05 (122.61)
V_2O_5[c]	HT	Monoclinic	$P2_1/m$	6.958 (7.114)	3.552 (3.561)	6.242 (6.284)	90.18 (90.07)
V_2O_5[d]	LT	Orthorhombic	Pmmn	11.573 (11.512)	3.544 (3.564)	4.23 (4.368)	90.00 (90.00)
V_2O_3[e]	HT	Hexagonal	$R\bar{3}c$	4.828 (4.925)	–	14.146 (13.837)	120.00 (120.00)
V_2O_3[f]	LT	Monoclinic	C2/c	7.494 (7.274)	4.690 (5.005)	5.737 (5.551)	96.78 (96.78)
V_3O_5[g]	HT	Monoclinic	C2/c	(9.846)	(5.027)	(7.009)	(109.536)
V_3O_5[h]	LT	Monoclinic	P2/c	9.831 (9.859)	4.986 (5.042)	6.997 (6.991)	109.47 (109.48)
V_4O_7[i]	HT	Triclinic	P$\bar{1}$	(5.509)	(7.008)	(12.256)	(95.10, 95.17, 109.2)
V_4O_7[i]	LT	Triclinic	P$\bar{1}$	5.537 (5.503)	6.696 (6.997)	11.931 (12.256)	94.30, 91.79, 106.71 (94.86, 95.16, 109.39)
V_6O_{13}[j]	HT	Monoclinic	C2/m	(11.922)	(3.680)	(10.138)	(100.87)
V_6O_{13}[k]	LT	Monoclinic	Pc	11.808 (11.963)	3.674 (3.711)	10.055 (10.060)	100.90 (100.92)

[a] Ref. [7].
[b] Ref. [8].
[c] Ref. [9].
[d] Ref. [10].
[e] Ref. [11].
[f] Ref. [12].
[g] Ref. [13].
[h] Ref. [14].
[i] Ref. [15].
[j] Ref. [16].
[k] Ref. [17].

extreme distortion. Virtually all bond angles deviate from the ideal angle of 90° and the bond lengths also vary for each surrounding atom. The distribution of both the bond lengths and angles within each compound are displayed in Fig. 2. As a result of the structural deformations, Fig. 2 shows a wide range of the length and angle distributions for most compounds. These distortions are known to occur in transition metal oxides, especially vanadium oxide, and have been suggested to be caused by second-order Jahn-Teller effects [58]. After closer examination of the structures, we have noticed an interesting result of these deformations. For the majority of compounds, if only the more closely bonded atoms are taken into account, the structures exhibit different geometric forms, as opposed to the typical octahedral coordination. V_2O_5 and V_6O_{13} are exemplary cases of this characteristic. For each of these two compounds (in either phase), the octahedra are distorted in a way that for each octahedron, one oxygen atom is greatly displaced away from the central vanadium atom, therefore causing the rest of the V—O bonds to exhibit square-pyramidal geometries. This displacement of certain atoms can also be seen in Fig. 2. It is clear that both V_2O_5 and V_6O_{13} contain a very wide range of bond lengths, and there exists strong outliers in the data. Excluding these outliers causes the V-coordination to appear more square-pyramidal, as opposed to octahedral. This agrees with previous reports which have found that V_2O_5 and V_6O_{13} consist of weakly bonded layers, made up of square-based pyramids, which interact mainly via Van der Waals bonding [16,17,35,59]. The structures of VO_2, V_2O_3, V_4O_7, and V_3O_5, display characteristics of both octahedral and tetrahedral coordinations, as shown in Fig. 1. Considering that the more closely bonded atoms will have a notably greater impact on the properties of the compound, these structural classifications will prove useful when discussing an explanation of the electronic structure of the materials. Eyert and Höck have studied V_2O_5 through *ab initio* methods, reported these types of structural distortions, and discussed their effect on the electronic structure of the compound [60]. Here, similar effects occur, in agreement with the results of Eyert and Höck for V_2O_5, and in many of the other compounds in this study.

The formation energies of each structure have been computed and listed in Table 2. Our results agree well with previous works reporting formation energies of certain vanadium oxides through *ab initio* methods [3,48]. For the compounds in this study, the normalized formation energies (E_{norm}) range from about −5.6 to −7.7 eV/O_2. The results indicate that high-temperature V_2O_3 is the most stable compound, whereas high-temperature V_2O_5 is the least. With regards to the MIT, there appears to be only a small difference between the formation energies of the high- and low-temperature phases for most compounds.

3.2. Charge transfer

Charge transfer has been computed for the high- and low-temperature phase of each compound. We define charge transfer as the amount of negative charge, in terms of elementary electronic charge ($-e$), which is transferred from vanadium to oxygen. The results show that for most compounds, charge transfer varies for each individual atom. The magnitude of the variation is largely dependent on the compound, as displayed in Fig. 3. Both VO_2 and V_2O_3 experience very little variation, while the rest of the compounds contain a much greater variety of charge transfer values. This behavior is especially the case for V_2O_5 and V_6O_{13}, which display the largest range of deviations. These two compounds also have the most disperse distribution of bond lengths and angles, as seen in Fig. 2. Conversely, VO_2 and V_2O_3, which both had relatively small bond length/angle deviations, display a very narrow range of charge transfer values. It appears that this correlation is consistent for all compounds reported here. The range of charge transfer is directly related to the level of bond length and angle variation. Therefore, we conclude that the charge transfer and crystal structure are closely linked. Additionally, Fig. 3 shows that there exist distinct groups of oxygen atoms within each compound which exhibit slightly unequal values of charge transfer. These are related to symmetrically in-equivalent types of oxygen positions within the structure. For example, the low-temperature phase of V_2O_5 contains three in-equivalent oxygen sites [10]
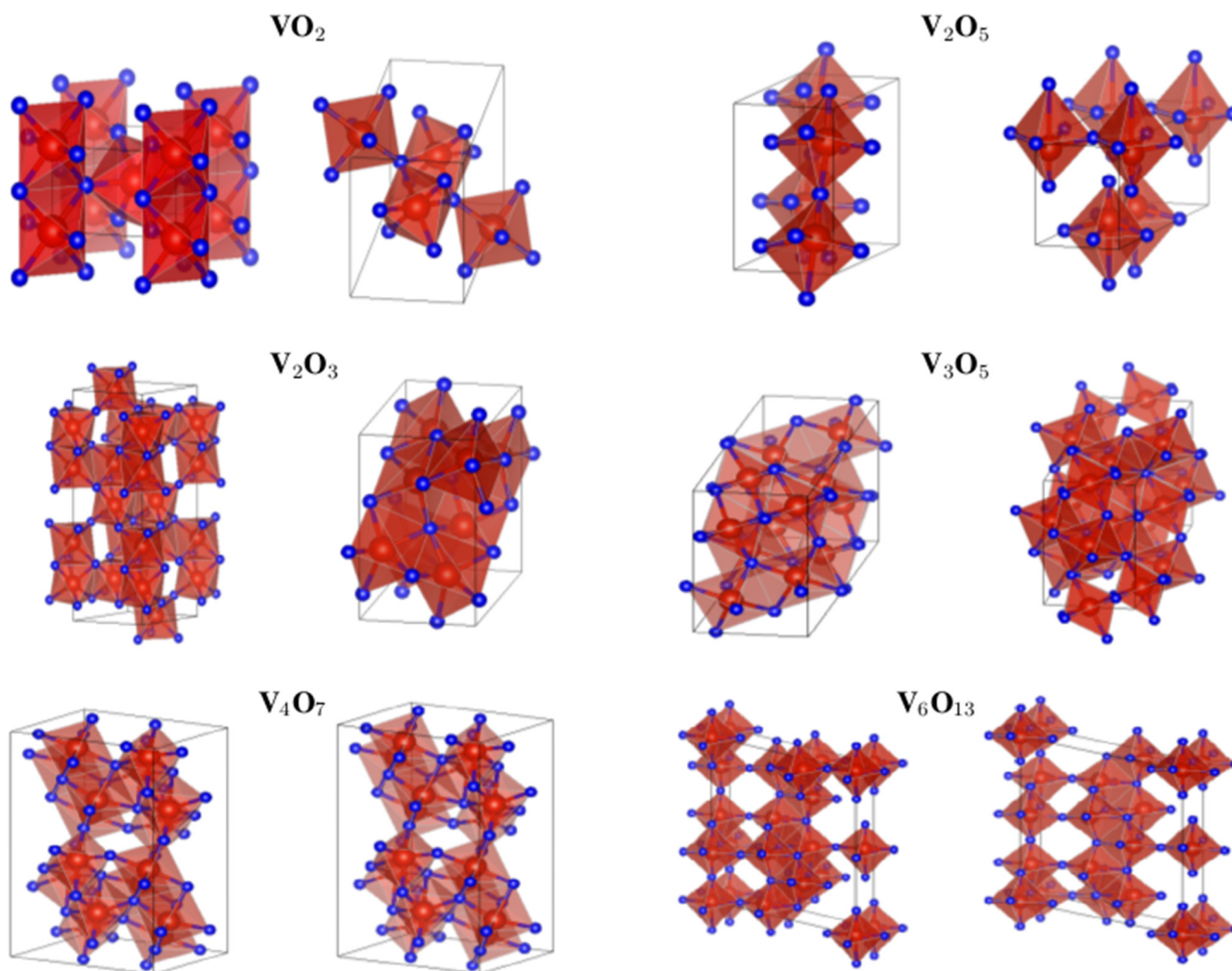
Fig. 1. Visual representations of the unit cell of each compound in the high- (left) and low-temperature (right) phase, as obtained through VESTA [73]. The blue points represent oxygen atoms, while the red points represent vanadium atoms. (For interpretation of the references to colour in this figure legend, the reader is referred to the web version of this article.)

resulting in three distinct groups of charge transfer values. Similar results occur for all other compounds in this work.

Average charge transfer values for each compound have also been calculated by analyzing the charge associated with each oxygen atom, determining the amount of negative charge each oxygen has received, and computing the arithmetic mean of these values. The results are displayed in Fig. 4 with exact values listed in Table S1 of the supplementary material. There is no consistent change in charge transfer over the MIT for the compounds in this work. For most compounds, there is almost zero difference between the charge transfer of the high- and low-temperature phases (<0.01 e). V_2O_3 and V_6O_{13} do exhibit some noticeable differences between the charge transfer of their high- and low-temperature phases, however the magnitude remains relatively small (0.01–0.05 e). Lastly, charge transfer as a function of vanadium to oxygen ratio is considered. The results show that for both the high- and low-temperature phases of all compounds, charge transfer decreases monotonically as a function of V-O ratio.

3.3. Electronic structure

We have calculated the electronic density of states for each compound through implementation of the hybrid HSE06 functional. From the resultant density of states, the band gaps were

computed for all compounds. Our calculated band gaps along with known experimental values are listed in Table 3. We have shown that the HSE06 functional provides a reasonably accurate prediction of band gap energies for almost all materials. The results show a great improvement in accuracy when compared to previous works which used solely the generalized gradient approximation (GGA) or local density approximation (LDA), both of which have resulted in underestimation of the band gaps [58,60,61]. These results also display an improvement over the GW method, which has been shown to slightly overestimate the gaps [33,35]. In a previous work, Guo and Robertson [5] have completed similar calculations by implementing hybrid functionals to compute the electronic structure for VO_2 and V_2O_3, resulting in band gaps of 0.53 and 0.6 eV respectively, which compare well with our results. For the low-temperature phase of V_4O_7, our calculated band gap does exhibit relatively large error as compared to experimental data, with a computed value of 0.83 eV versus the experimental value of 0.1 eV [22]. However, this over-estimation is consistent with earlier computational work of Botana et al., in which LDA + U was implemented, resulting in a band gap of 0.6 eV for the low-temperature phase of V_4O_7 [30].

We have also tested the accuracy of GGA + U when used to determine the electronic structure of vanadium oxides. We used a U-value of 3.25 eV, as recommended by Wang et al. [48]. The
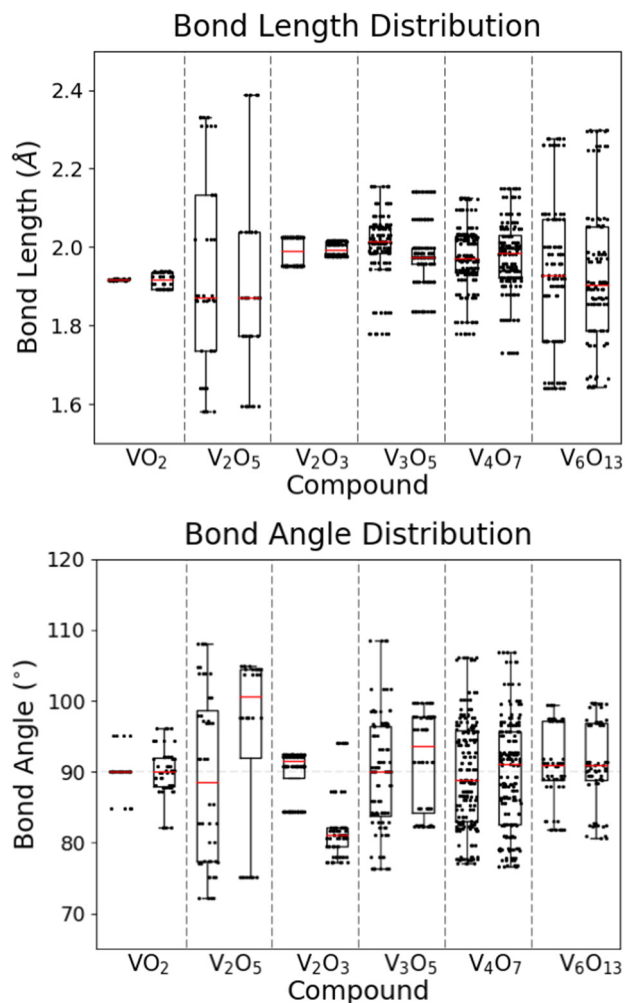
Bond Length Distribution

Bond Angle Distribution

Fig. 2. The distribution of bond lengths and angles for all materials in this study. Each compound is shown in both the high- (left) and low-temperature (right) phase. Each dot represents a V—O bond length or O—V—O bond angle within the unit cell. The median value of the lengths/angles is shown by the red lines. The boxes extend from the lower to upper quartile values of the data, whereas the whiskers extend to show the range of the data. (For interpretation of the references to colour in this figure legend, the reader is referred to the web version of this article.)

Charge Transfer Distribution

Fig. 3. The distribution of charge transfer, in units of elementary electronic charge ($-e$), from vanadium to oxygen, for each compound in the high- (left) and low-temperature (right) phase. Each dot represents the amount of negative charge which each individual oxygen atom is receiving. The median value of charge transfer in each compound is shown by the red lines. The boxes extend from the lower to upper quartile values of the data, whereas whiskers extend to show the range of the plot. (For interpretation of the references to colour in this figure legend, the reader is referred to the web version of this article.)

Charge Transfer vs. V-O Ratio

Fig. 4. The average values of charge transfer, in units of elementary electronic charge ($-e$), from vanadium to oxygen, as a function of V-O ratio.

Table 2
Normalized formation energies of each compound in both the high- and low-temperature phase, represented by "HT" and "LT". The values shown are in units of eV/O$_2$, where O$_2$ represents the number of oxygen molecules within the unit cell of each compound.

Compound	Phase	E_{norm} (eV/O$_2$)
VO$_2$	HT	−7.162
VO$_2$	LT	−7.158
V$_2$O$_5$	HT	−6.370
V$_2$O$_5$	LT	−6.458
V$_2$O$_3$	HT	−7.682
V$_2$O$_3$	LT	−7.118
V$_3$O$_5$	HT	−7.635
V$_3$O$_5$	LT	−7.532
V$_4$O$_7$	HT	−7.601
V$_4$O$_7$	LT	−7.592
V$_6$O$_{13}$	HT	−6.982
V$_6$O$_{13}$	LT	−6.981

densities of states derived from GGA + U are qualitatively very similar to the densities derived from hybrid functionals for all compounds in this study. How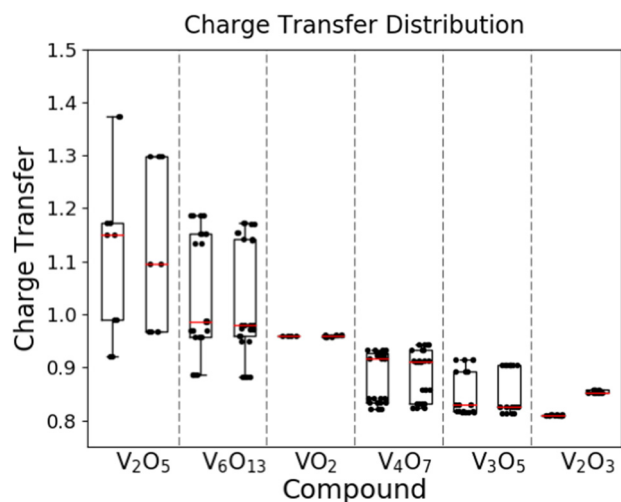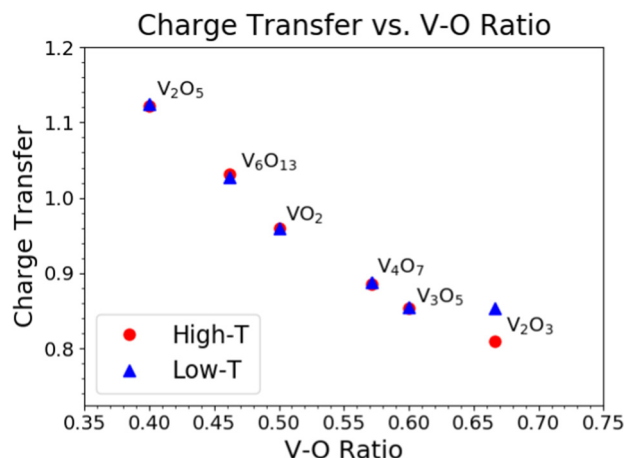ever, the magnitude of the computed band gap does vary substantially depending on the method used. Our results show that GGA + U results in a consistent underestimation of the band gap. Therefore, we conclude that hybrid functionals provide a more reliable *ab initio* method to determine the band gap energies of vanadium oxides and possibly for similar materials.

Despite the shortcomings of GGA + U with respect to the prediction of band gaps, we found that this method yields optical properties which are much closer to those reported in experimental work [21–24] when compared to results found through our use of hybrid functionals. Therefore, in Fig. 5, we show the projected density of states for each compound, as found with the GGA + U method. The results for each compound show that the p orbital states are filled i.e. are below the E$_f$, while the d orbital states are unfilled, as expected. The d orbital states have been plotted in their t_{2g}/t_g and e_g components. The t_{2g}/t_g densities represent the sum of the d_{xy}, d_{yz}, and d_{xz} states, and the e_g densities represent the sum of the d_{x2-y2} and d_{z2} states. As according to convention, we use t_{2g} for octahedral and square pyramidal coordination, and t_g for tetrahedral coordination. The energy positioning of the t_{2g}/t_g and e_g

Table 3
Electronic band gap energy values for each compound obtained though HSE06 calculations, along with experimental values from the literature for comparison. "HT" and "LT" represent the high- and low-temperature phase. *Experimental data for the band gap of the high-temperature phase of this compound is limited.

Compound	Phase	Exp. Band Gap (eV)	Calc. Band Gap (eV)
VO_2	HT	0.00	0.00
VO_2	LT	0.60[a]	0.66
V_2O_5	HT	*	2.32
V_2O_5	LT	2.35[b]	2.62
V_2O_3	HT	0.00	0.00
V_2O_3	LT	0.66[c]	0.78
V_3O_5	HT	0.00	0.00
V_3O_5	LT	0.62[d]	0.55
V_4O_7	HT	0.00	0.00
V_4O_7	LT	0.10[e]	0.83
V_6O_{13}	HT	0.00	0.00
V_6O_{13}	LT	0.20[f]	0.17

[a] Ref. [18].
[b] Ref. [19].
[c] Ref. [20].
[d] Ref. [21].
[e] Ref. [22].
[f] Ref. [23].

orbitals shows mixed results which depend strongly on the compound. These characteristics can be interpreted as resulting from the molecular geometries. Typically, crystal field splitting is known to cause separation of the t_{2g}/t_g and e_g orbitals [62]. For compounds with octahedral or square pyramidal coordination, the t_{2g} orbitals tend to occupy the lower energies, while the e_g orbitals lie higher [62]. Square pyramidal coordination causes a larger separation of t_{2g} and e_g orbitals as compared to octahedral coordination [62]. Conversely, tetrahedral geometry leads to an opposite effect, where the t_g orbitals have a higher energy than the e_g orbitals, although the separation is relatively small [62]. Other molecular coordination types also cause splitting, but generally exhibit more mixing of the t_{2g}/t_g and e_g orbitals [58]. As discussed earlier, the majority of compounds are distorted in such a way that they exhibit more than one type of geometry, which helps to explain their electronic structures. The two compounds which exhibit the most prominent splitting of orbitals are V_2O_5 and V_6O_{13}. In each, the e_g bands lie higher in energy than the t_{2g} bands. This observation correlates with the structures of V_2O_5 and V_6O_{13}, which exhibit square pyramidal coordination. One other compound which experiences noticeable splitting (although to a lesser degree), is the high-temperature phase of V_2O_3. However, for this compound, the t_g bands occur above the e_g bands. This behavior indicates that the high-temperature V_2O_3 exhibits properties corresponding to a tetrahedral geometry, which agrees with our analysis of the structure in Section 3.1. Similar effects occur for the low-temperature phase of VO_2. For much of the rest of the compounds, the orbitals appear to be mostly mixed, which is most likely due to multiple underlying structural characteristics which cause opposing effects. Consider the properties of V_4O_7 as an example. Its structure appears to exhibit both octahedral and tetrahedral properties, as stated previously in Section 3.1. It is known that these two molecular coordinations have opposite effects on the energy positioning of the t_{2g}/t_g and e_g orbitals [62]. Therefore, the result is strong blending of the orbitals, with no clear separation. Thus, the projected density of states provides further evidence that it may be more proper to characterize the structures of vanadium oxides as forms different from typical octahedral coordination.

3.4. Optical properties

The optical calculations were initially performed using hybrid functionals, the results of which are shown in Figs. S1 and S2 of the supplementary material. Although this method gave an accurate description of band gap energies for the most compounds in this study, the results for the complex dielectric function were in very poor agreement with experimental measurements [22,24–27]. The general pattern of the calculated optical conductivity was fairly similar to experimental data, but the photon energy values at which specific features occur are shifted significantly to higher energies. This type of discrepancy in optical properties of vanadium oxides is consistent with previous theoretical results found using hybrid HSE06 functionals for VO_2 [31,32] and the GW approximation for V_2O_5 [35]. It is known that electron-hole interaction and lattice polarization each cause dielectric spectra to be shifted towards lower energies [63–65]. Standard hybrid functionals do not account for these effects, and therefore tend to overestimate the energies at which absorption peaks occur [66]. Typically, the error is relatively small; silicon, for example, exhibits a shift of about 0.5 eV [67]. However, for materials which exhibit strong interaction and/or polarization, the discrepancy becomes substantial. Computed dielectric functions for compounds such as LiF, NaCl, and AlN have been shown to overestimate the absorption peaks by 3–4 eV [65,67]. Therefore, we conclude that our results indicate strong electron-hole interaction and lattice polarization within the systems.

Considering this issue with hybrid functionals, we also computed optical properties with the GGA + U method. Since the *U*-value is chosen based on experimental data, this method should better account for the strong electron-hole interaction and lattice polarization within these compounds. The resultant complex dielectric function spectra are displayed in Fig. S3 of the supplementary material. Due to the anisotropic nature of the compounds, ε_1 and ε_2 are plotted in their directional (*x*, *y*, and *z*) components. For compounds with monoclinic or triclinic geometries, off-diagonal elements of the dielectric tensor are also shown. Here, we focus on the property of optical conductivity, which is most widely studied in the literature. Fig. 6 shows the comparison between the calculated and experimental optical conductivities for all compounds in this study, with the exception of high-temperature V_2O_5, as it has not been experimentally reported, most likely due to its high critical temperature of 530 K. Therefore, a purely predictive description for the optical conductivity of this compound is provided. For the remaining compounds, the features of the conductivity match with experimental data qualitatively well. The results appear to closely coincide with experimental data in the cases of VO_2, V_2O_5, and V_2O_3, but this degree of correlation changes for the remaining three compounds. The calculated optical conductivities of V_3O_5, V_4O_7, and V_6O_{13} display much greater disagreement with experimental data, as opposed to the first three compounds. One potential cause for this difference could be the choice of the *U*-value used throughout the calculations. In the work of Wang et al., only VO_2, V_2O_5, and V_2O_3 were taken into account when determining the most effective *U*-value to use for vanadium oxide compounds. This was a reasonable choice, given that these three compounds are the most common of the vanadium oxides. We suggest that further investigation into this problem could be beneficial. Determining a proper *U*-value through a more refined approach, such as considering the coordination sphere around the cation, would be a likely solution [68,69].

Further analysis reveals another noticeable pattern, which is the failure of the theoretical results to predict any substantial rise in the optical conductivity of metallic compounds at low frequencies. According to Drude theory for metals, the imaginary part of the dielectric function (ε_2) should approach infinity as photon frequency approaches zero (which is known as the Drude tail) [70]. Optical conductivity is directly related to ε_2, and should therefore rise substantially at low frequencies. This phenomenon is observed in the experimental data [22,24–27]. In vanadium oxides, the
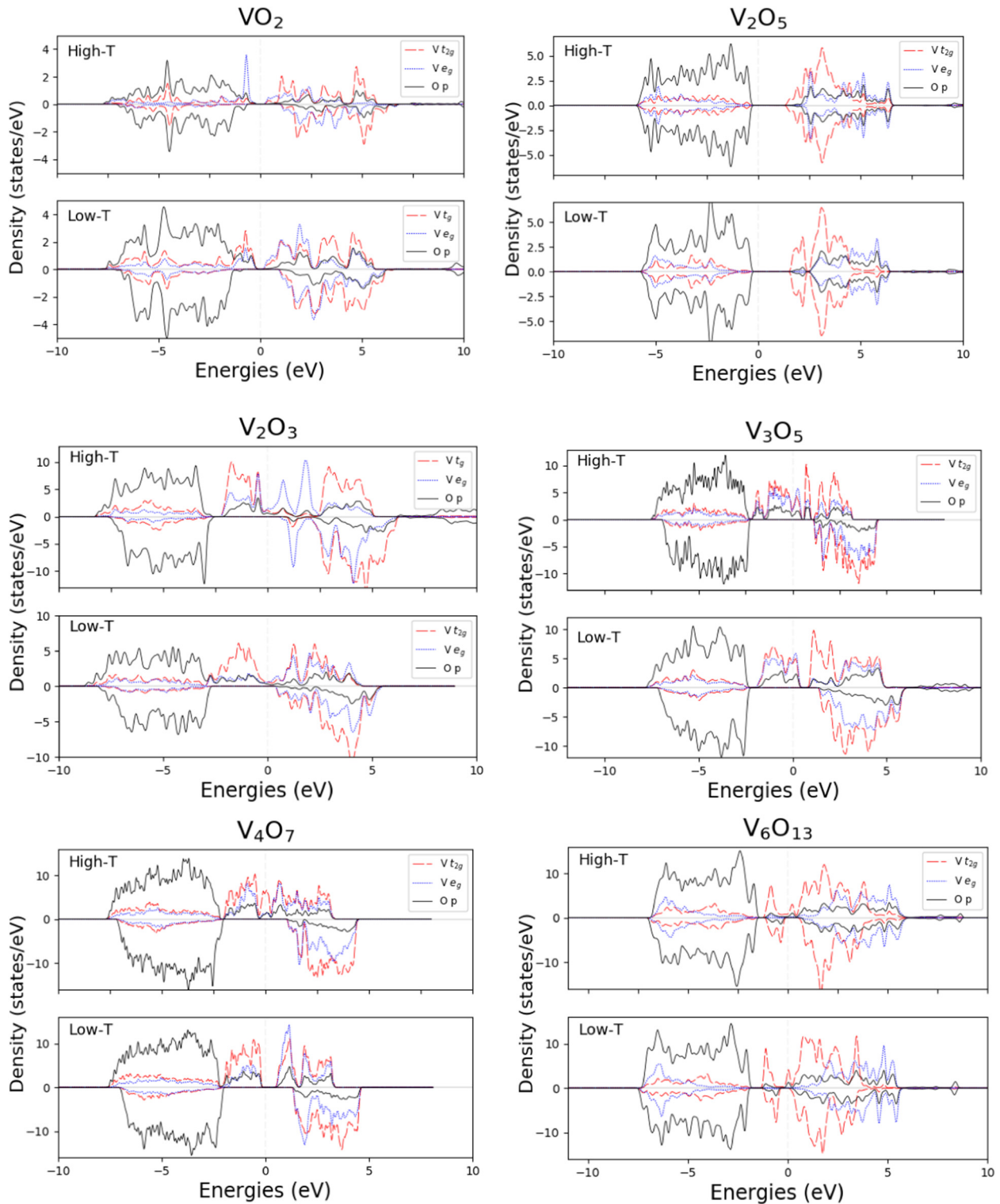
Fig. 5. Density of states, as calculated through the GGA + U method with a *U*-value of 3.25 eV. Spin-up densities are represented by positive values are plotted above the y-axis. Spin-down densities are represented by negative values are plotted below. The Fermi energy of each compound is set to 0 eV. Vanadium electrons occupy the *d* orbitals, which are plotted in their t_{2g}/t_g and e_g components. Oxygen electrons occupy the *p* orbitals, and are plotted as such.

Drude tail is typically attributed to free carrier absorption and *d-d* intraband transitions [71]. Since our optical conductivity as derived from GGA + U fails to predict the Drude tail, we computed optical conductivity with decreasing *U*-values and analyzed the results. We found that there was a direct inverse correlation between the implemented *U*-value and the magnitude of the Drude tail. Decreasing the *U*-value caused an increase in the conductivity at low frequencies. Standard GGA calculations (zero *U*-value) resulted in the greatest rise in conductivity as frequency approached zero. Therefore, we conclude that the addition of the
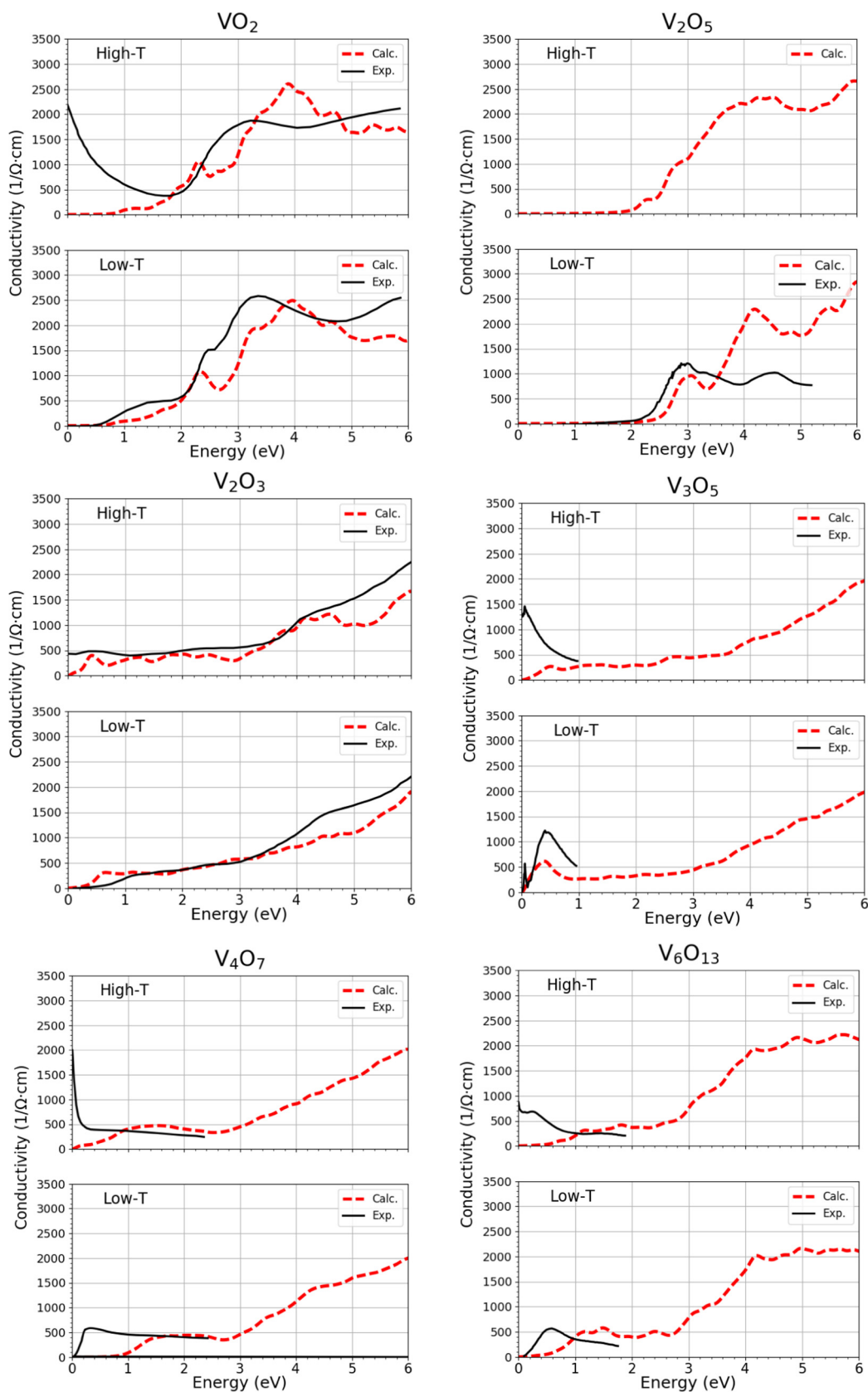
Fig. 6. Optical conductivity of each compound, obtained through implementation of the GGA + U method with a *U*-value of 3.25 eV. Both the calculated and experimental results are plotted as a function of photon energy, ranging from 0 to 6 eV. Due to the anisotropic nature of the materials, we have calculated the average of the conductivity in the three dimensions and used these resulting values in order to compare with experimental data. However, the individual directional components can be viewed in the supplementary material. Experimental data was adopted from the following sources: VO$_2$ Ref. [24], low-temperature V$_2$O$_5$ Ref. [25], V$_2$O$_3$ Ref. [24], V$_3$O$_5$ Ref. [26], V$_4$O$_7$ Ref. [22], and V$_6$O$_{13}$ Ref. [27].

U-value causes a reduction in strength of free carrier absorption and *d-d* intraband transitions for the metallic compounds in this study.

4. Conclusion

Structural, electronic, and optical properties of VO_2, V_2O_5, V_2O_3, V_3O_5, V_4O_7, and V_6O_{13} in their low- and high-temperature variants have been obtained using first principles computational methods. Examination of the structures has shown that many of the compounds in this study exhibit a strong distortion of their octahedral complexes. These distortions lead us to believe that many of the compounds should be considered to exhibit various other molecular geometries, as opposed to simply classifying them as having octahedral coordination.

Bader's analysis quantified charge transfer for each compound over the MIT. The magnitude of the charge transfer appears to be closely tied to the underlying structure within each phase. The results show no consistency in change of charge transfer over the transition, therefore leading us to believe that charge transfer plays little to no role in the MIT. The charge transfer is also shown to decrease monotonically as V-O ratio increases for all compounds.

Hybrid functionals are capable of accurately predicting the band gap of the majority of compounds in this study, which provides evidence that this method could be used for electronic structure calculations of other strongly correlated materials. The GGA + U method has also been implemented to describe the electronic structure of the compounds. The partial density of states, computed with GGA + U, supports our hypothesis regarding the structural characteristics of the system, as results show the energy positioning of the t_{2g} and e_g orbitals deviates substantially from the expected characteristics of compounds with octahedral structures.

Complex dielectric function and complex optical conductivity spectra have been computed using both hybrid functionals and the GGA + U method. The results have shown that although the hybrid functionals give an accurate prediction of band gap energies, they are unable to predict the optical properties of the compounds to the same degree of accuracy. As compared with our computed values, the experimental dielectric spectra are shifted substantially towards lower energies, implying strong electron-hole interaction and lattice polarization within the systems. The GGA + U method provides a much better description of optical properties for vanadium oxides. Based on the pattern of discrepancies in the optical conductivity, we propose the potential project of determining a more suitable *U*-value for V_3O_5, V_4O_7, and V_6O_{13}. We also suggest that the addition of the *U*-value causes a large reduction of free carrier absorption and *d-d* intraband transitions, therefore failing to predict a characteristic Drude tail for the metallic compounds.

Appendix A. Supplementary material

Supplementary data associated with this article can be found, in the online version, at https://doi.org/10.1016/j.commatsci.2018.01.048.

References

[1] C.N.R. Rao, Annu. Rev. Phys. Chem. 40 (1989) 291.
[2] S. Lany, J. Phys.: Condens. Matter. 27 (2015) 283203.
[3] C. Wu, F. Feng, Y. Xie, Chem. Soc. Rev. 42 (2013) 5157.
[4] E.E. Chain, Appl. Opt. 30 (1991) 2782.
[5] Y. Guo, J. Robertson, Micro. Eng. 109 (2013) 278.
[6] M. Imada, A. Fujimori, Y. Tokura, Rev. Mod. Phys. 70 (1998) 1039.
[7] S. Westman, Acta Chem. Scand. 15 (1961) 217.
[8] G. Andersson, Acta Chem. Scand. 10 (1956) 623.
[9] V.P. Filonenko, M. Sundberg, P.E. Werner, I.P. Zibrov, Acta Crystallogr. B. 60 (2004) 375.
[10] R. Enjalbert, J. Galy, Acta Crstallogr. C. 42 (1986) 1467.
[11] R.E. Newnham, Y.M. de Haan, Z. Kristallogr. 117 (1962) 235.
[12] C. Tenailleau et al., J. Solid State Chem. 174 (2003) 431.
[13] S.-H. Hong, S. Asbrink, Acta Crystallogr. 38 (1982) 713.
[14] S. Asbrink, Acta Crystallogr. 36 (1980) 1332.
[15] J.-L. Hodeau, M. Marezio, J. Solid State Chem. 23 (1978) 253.
[16] K.-A. Willhelmi, K. Waltersson, L. Kihlborg, Acta Chem. Scand. 25 (1971) 2675.
[17] J. Höwing, T. Gustafsson, J.O. Thomas, Acta Crystallogr. 59 (2003) 747.
[18] T.C. Koethe et al., Phys. Rev. Lett. 97 (2006) 116402.
[19] N. Van Hieu, D. Lichtman, J. Vac. Sci. Technol. 18 (1981) 49.
[20] G.A. Thomas et al., Phys. Rev. Lett. 73 (1994) 1529.
[21] E.I. Terukov, D.I. Khomskii, F.A. Chudnovskii, Sov. Phys. JETP. 46 (1977) 1160.
[22] I. Lo Vecchio et al., Phys. Rev. B. 90 (2014) 115149.
[23] R. Eguchi, T. Yokoya, T. Kiss, Y. Ueda, S. Shin, Phys. Rev. B. 65 (2002) 205124.
[24] M.M. Qazilbash et al., Phys. Rev. B. 77 (2008) 115121.
[25] T.D. Kang, J.-S. Chung, J.-G. Yoon, Phys. Rev. B. 89 (2014) 094201.
[26] L. Baldassarre et al., Phys. Rev. B. 75 (2007) 245108.
[27] A. Irizawa et al., J. Electron. Spectrosc. Relat. Phenom. 144 (2005) 345.
[28] A.J. Cohen, P. Mori-Sanchez, W. Yang, Science. 321 (2008) 792.
[29] T. Toriyama, T. Nakayama, T. Konishi, Y. Ohta, Phys. Rev. B. 90 (2014) 085131.
[30] A.S. Botana, V. Pardo, D. Baldomir, A.V. Ushakov, D.I. Khomskii, Phys. Rev. B. 84 (2011) 115138.
[31] A. Gali, J.E. Coulter, E. Manousakis. Available from: <arXiv:1207.6098>.
[32] J.E. Coulter, E. Manousakis, A. Gali, Phy. Rev. B. 90 (2014) 165142.
[33] S. Kobayashi, Y. Nohara, S. Yamamoto, T. Fujiwara, Phys. Rev. B. 78 (2008) 155112.
[34] Y. Guo, S.J. Clark, J. Robertson, J. Chem. Phys. 140 (2014) 054702.
[35] C. Bhandari, W.R.L. Lambrecht, M. van Schilfgaarde, Phys. Rev. B. 91 (2015) 125116.
[36] V.V. Porsev, A.V. Bandura, R.A. Evarestov, Acta Materialia. 75 (2014) 246.
[37] G. Kresse, J. Hafner, Phys. Rev. B. 47 (1993) 558.
[38] G. Kresse, J. Hafner, Phys. Rev. B. 49 (1994) 14251.
[39] G. Kresse, J. Furthmüller, Comput. Mat. Sci. 6 (1996) 15.
[40] G. Kresse, J. Furthmüller, Phys. Rev. B. 54 (1996) 11169.
[41] P.E. Blöchl, Phys. Rev. B. 50 (1994) 17953.
[42] G. Kresse, D. Joubert, Phys. Rev. B. 59 (1999) 1758.
[43] I. Efthimiopoulos et al., J. Phys. Chem. A. 118 (2014) 1713.
[44] W. Tang, E. Sanville, G. Henkelman, J. Phys. Condens. Matter. 21 (2009) 084204.
[45] S.L. Dudarev et al., Phys. Rev. B 57 (1998) 1505.
[46] V.A. Ranea, P.L. Damming Quiña, Mater. Res. Express 3 (2016) 085005.
[47] M.V. Ganduglia-Pirovano, A. Hofmann, J. Sauer, Surf. Sci. Rep. 62 (2007) 219.
[48] L. Wang, T. Maxisch, G. Ceder, Phys. Rev. B. 73 (2006) 195107.
[49] J. Hubbard, Proc. A. 276 (1963) 238.
[50] M. Gajdoš, K. Hummer, G. Kresse, J. Furthmüller, F. Bechstedt, Phys. Rev. B. 73 (2006) 045112.
[51] R. Deng, B.D. Ozsdolay, P.Y. Zheng, S.V. Khare, D. Gall, Phys. Rev. B. 91 (2015) 045104.
[52] D.J. Griffiths, R. College, Introduction to Electrodynamics, Prentice Hall, New Jersey, 1999.
[53] Z.T.Y. Liu, X. Zhou, S.V. Khare, D. Gall, J. Phys. Condens. Matter. 26 (2014) 25404.
[54] Z.T.Y. Liu, B.P. Burton, S.V. Khare, P. Sarin, Comput. Mater. Sci. 443 (2016) 137.
[55] L.F. Mattheiss, J. Phys. Condens. Matter. 6 (1994) 6477.
[56] C. Lamsal, N.M. Ravindra, JOM. 67 (2015) 3022.
[57] T.J. Giese, D.M. York, J. Chem. Phys. 133 (2010) 244107.
[58] K.M. Ok, P. Shiv Halasyamani, Chem. Mater. 18 (2006) 3176.
[59] E. Londero, E. Schröder, Phys. Rev. B 82 (2010) 054116.
[60] V. Eyert, K.-H. Höck, Phys. Rev. B. 57 (1998) 12727.
[61] V. Eyert, Ann. Phys. (Leipzig). 11 (2002) 650.
[62] J.J. Zuckerman, J. Chem. Educ. 42 (1965) 315.
[63] W. Hanke, L.J. Sham, Phys. Rev. B. 21 (1980) 4656.
[64] G. Bussi, Physica Scripta. 109 (2004) 141.
[65] F. Bechstedt, K. Seino, P.H. Hahn, W.G. Schmidt, Phys. Rev. B. 72 (2005) 245114.
[66] J. Paier, M. Marsman, G. Kresse, Phys. Rev. B. 78 (2008).
[67] M. Rohlfing, S.G. Louie, Phys. Rev. B. 62 (2000) 4927.
[68] V. Stevanovic, S. Lany, X.W. Zhang, A. Zunger, Phys. Rev. B. 85 (2012) 115104.
[69] M. Aykol, C. Wolverton, Phys. Rev. B. 90 (2014) 115105.
[70] P. Drude, Ann. Phys.–Berlin 306 (1900) 566.
[71] R.J.O. Mossanek, M. Abbate, J. Phys. Condens. Matter. 19 (2007) 346225.
[72] Ohio-Supercomputer-Center, 1987. <http://osc.edu/ark:/19495/f5s1ph73>.
[73] K. Momma, F. Izumi, J. Appl. Crystallogr. 44 (2011) 1272.